Supplementary Information for

Unveiling the hidden viral biodiversity and potential ecological functions with Global Coral Holobiont Virome Database

This file includes:

Supplementary Results

Supplementary Discussions

Supplementary Figures 1 to 22

Supplementary Results

Text 1 (results)

The interactions between coral viruses and their host

For bacterial mOTUs, they were distributed across 41 phyla, Pseudomonadota was the most abundant (554 mOTUs), followed by Bacteroidota (224 mOTUs) and Cyanobacteriota (48 mOTUs). In contrast, archaeal mOTUs were less diverse, covering only 5 phyla, and were dominated by Thermoproteota (19 mOTUs) and Thermoplasmatota (7 mOTUs) (Data S10 and Supplementary Figure 13). To further understand the ecological distribution of these microbial communities, we compared their composition across healthy, bleached, and diseased corals. We found that the bacterial community structure remained relatively consistent across health states, with Bacteroidota being the most abundant phylum, followed by Cyanobacteriota and Pseudomonadota (Supplementary Figure 14). In contrast, archaeal communities exhibited health-state specificity, with Asgardarchaeota predominantly associated with healthy samples and Thermoproteota enriched in bleached and diseased individuals (Supplementary Figure 14).

Specifically for bacterial communities, most species were dominated by Cyanobacteriota, Bacteroidota, and Pseudomonadota, while *Montastraea caverosa* (MC), *Plerogyra sinuosa* (PLS), *Pavona varians* (PAV), and *Orbicella faveolata* (OF) were dominated by Spirochaetota (Supplementary Figure 16). Archaeal communities also varied by coral species, most were dominated by Halobacteriota, Asgardarchaeota, and Thermoproteota, whiel *Pocillopora verrucosa* (PV), *Pocillopora* (PO), and *Meandrina meandrites* (MM) were dominated by Nanoarchaeota (Supplementary Figure 16).

Text 2 (results)

Mapping vAMGs to genomic contigs can help us further revealed multiple vAMGs involved in diverse metabolic pathways within individual viral genomes (Supplementary Figure 17). Most of these viruses belonged to Caudoviricetes, with a smaller proportion in Megaviricetes. For example, the *Pst* gene family mapped to module 1 of vOTU3, a core module aiding virus-host adaptation to P starvation, particularly in low-P environments. Fe metabolism/transport genes (*feoA*/*feoB* and *exbB*/*exbD*) were detected in vOTU6, vOTU8, vOTU21, and vOTU86, revealing these viruses may strengthen host interactions *via* regulating Fe metabolic networks. The *Nir* gene family mapped to module 1 of vOTU4 and was involved in denitrification regulation. Within vOTU23, genes for sulfate reduction (*dsrC*/*dsrA*/*dsrB*), S transport (*tusA*/*tusB*), and sulfite reduction (*aprB*/*aprA*) indicated multifunctional roles in S metabolism. C metabolism genes (*nagZ* and *murG*) mapped to vOTU193 and vOTU86 (Megaviricetes). Additionally, CH_4 metabolism-associated *Rnf* and *Por* families corresponded to vOTU4, vOTU40, and vOTU193, suggesting potential viral intervention in host CH_4 metabolism (Supplementary Figure 17).

To explore vAMG functional mechanisms, we predicted 3D protein structures of six key vAMGs (*nagZ, glnA, acs, phoH, cysK,* and *fecA*) using the PDB database (Supplementary Figure 17). Results showed the *nagZ* gene (involved in C metabolism) has a typical β-1,4-glucosidase catalytic domain in tertiary structure, with catalytic residues Glu205 and Glu358

that hydrolyze terminal N-acetylglucosamine in chitin oligosaccharides, which provides a structural basis for viral utilization of host carbohydrates. For the N-metabolic member, *glnA* gene (vOTU5: region1) features a highly conserved ATP-binding domain in the central α/β-fold, this domain stably interacts with ATP *via* Lys285 and Asp324 to supply the phosphorylation energy required for glutamine synthesis. The 3D structure of *acs* (vOTU1: region1) includes a coenzyme A-binding domain that ensures substrate recognition and catalytic efficiency in acetyl-CoA synthesis. As for the P metabolic element, the *phoH* gene (vOTU1: region11) contains a signal transduction domain with phosphorylation sites on the protein surface, which responds to changes in environmental phosphate concentration to activate downstream phosphate metabolism genes. Into the S metabolic gene, *cysK* (vOTU3: region2) includes a sulfide-binding domain, a sulfurophilic pocket in the protein center that specifically binds sulfides to ensure the S supply for cysteine synthesis. The last gene related with Fe metabolism (*fecA* gene) (vOTU10: region2) has a typical TonB-dependent outer membrane receptor domain consisting of a 22-stranded β-barrel transmembrane structure and an N-terminal plug domain; its surface Fe (III)-enterobactin binding site, composed of Asp192, Tyr193, and His207 residues, specifically recognizes and transports siderophore complexes from the host environment. These structural predictions provide critical insights into the functions of vAMGs in virus-host interactions (Supplementary Figure 18).

Supplementary Discussions

Text 1 (discussions)

While our bioinformatic thresholds were adjusted to be less stringent than the widely accepted community guidelines (Roux et al.[1] and Bowers et al.[2]), this modification was deliberate to balance two key objectives: retaining ecologically meaningful viral sequences (such as low-abundance or fragmented genomes that are prevalent in coral holobiont samples) and upholding rigorous data quality. To mitigate potential biases associated with this adjustment, we integrated targeted quality control and statistical correction steps into our analytical pipeline. For MAGs with a maximum allowed contamination of 20%, we validated the authenticity of predicted prophages by confirming the presence of bacterial flanking regions (e.g., host genomic sequences upstream and downstream of the prophage integration site) through a combination of VirSorter2 analysis[3] and manual curation, this step effectively reduced false positives stemming from binning errors, as integrated prophages typically retain such flanking sequences that distinguish them from spurious viral-like fragments[3]. Prior to virus-host association analyses, we used CheckV (v1.0.1)[4] to assess viral contig quality, removing those with contamination scores >5% and retaining only high-quality draft and finished genomes that conform to MIUViG standards[1] for uncultivated viral genomes (UViGs). This step ensured that the viral sequences used for host alignment were free of host genomic contaminants. Additionally, for the Spearman's rank correlations employed in cooccurrence network analyses, we supplemented the original approach with Benjamini-Hochberg (BH) correction to control the false discovery rate (FDR), setting an adjusted *P*-value threshold of < 0.05. Critical cooccurrence patterns (e.g., core virus-host pairs) remained consistent after correction, confirming the robustness of our main findings against biases arising from uncorrected multiple comparisons.

Despite these safeguards, we acknowledge inherent limitations associated with relaxed thresholds. For instance, fragmented viral genomes (<10 kb) may still be incorporated into downstream analyses. Consistent with MIUViG guidelines, such sequences demand cautious interpretation[3], and we have alleviated this concern by excluding contigs that lack at least one viral hallmark gene (e.g., capsid proteins, terminases) and confining functional annotations to conserved, well-characterized genes. Additionally, while BH correction reduces Type I errors (false positives), it may marginally increase Type II errors (false negatives) for weak yet biologically meaningful correlations. Future studies leveraging expanded sample sizes, stricter filtering criteria, and refined analytical approaches could help clarify these interactions and mitigate the trade-offs inherent in threshold adjustments.

The coral holobiont, comprising coral animals, symbiotic algae, and diverse microorganisms, provides exclusive host resources for viruses, supporting the persistence and diversification of viral lineages[5]. Moreover, the relatively stable temperature, light, and nutrient conditions within coral reef ecosystems further select for viral taxa adapted to such environments, thereby limiting genetic exchange with viruses from other habitats and ultimately leading to the formation of highly specialized viral communities[6,7]. Community structure analysis further revealed strong host type dependence in viral composition, accompanied by distinct biogeographic trends linked to latitude.

The observed latitudinal patterns in both α and β diversity provide valuable insights into the biogeographic dynamics of virus-microbe communities. The significantly higher α-diversity in middle-latitude regions, compared with low and high latitudes (Fig. 2A), suggests that middle latitudes may offer a more favorable combination of environmental factors (such as temperature, precipitation, and resource availability) that promote the coexistence and proliferation of a wider range of viral and microbial taxa[8]. This aligns with the idea of a "latitudinal diversity peak" often observed in various ecological systems, where moderate environmental conditions support greater biodiversity. For β-diversity, the significant differences between latitudes for both vOTUs and mOTUs indicate that geographic distance associated with latitude is a key driver of community dissimilarity (Fig. 2B). These biogeographic patterns mirror those observed in intertidal and soil viromes[9,10], where viral and microbial communities exhibit highly convergent spatial distributions, underscoring the tight ecological coupling between viruses and their microbial hosts. In coral reefs, these mid-latitude conditions potentially involve moderate temperature fluctuations, balanced nutrient availability, and optimal host physiological homeostasis, collectively fostering the coexistence and diversification of both viruses and microorganisms.

Text 2 (discussions)

For instance, Artverviricota targeted Flavobacteriaceae and Flammeovirgaceae (Fig. 3D). These two bacterial families are mainly involved in polysaccharide degradation and nutrient cycling, which suggests that Artverviricota plays a specialized role in modulating core metabolic taxa. In contrast, Uroviricota displayed a broad host range, spanning distantly related bacterial lineages (Pseudomonadota) and archaeal groups (Asgardarchaeota), indicative of a generalist

strategy (Fig. 3D and Data S12). This breadth may confer resilience under fluctuating environmental conditions (e.g., temperature shifts or nutrient pulses), allowing generalist viruses to maintain regulatory influence even as host community composition changes, thereby ensuring functional continuity and ecosystem stability. Additionally, it should be noted that previous study has also examined the metagenome of coral symbionts to a limited extent, such as Wallace et al.[11]. However, our work differs from them in several respects. Wallace et al.[11] mainly focused on *Orbicella faveolata* and other *Caribbean* stony corals, whose microbiomes are well-documented to be dominated by Alphaproteobacteria. In contrast, our meta-analysis included a broader range of coral species (e.g., Indo-Pacific branching and massive corals) that harbor distinct core microbiomes, many of which rely on Bacteroidota for organic matter degradation and Cyanobacteriota for photosynthetic nutrient supply. This aligns with the well-established paradigm that coral species identity is a primary driver of microbiome composition, which in turn shapes viral host preference. Notably, these differences do not contradict Wallace et al.[11] but rather highlight the context dependency of virus-host interactions in coral holobionts. Both studies confirm that coral-associated viruses exhibit strong host phylum specificity, with viral communities tightly linked to the taxonomic composition of their bacterial hosts, reinforcing the role of viruses as key regulators of coral microbiome structure[12]. The convergence of methodological approaches across studies further validates the robustness of virus-host assignment *via* CRISPR-provirus matching. The divergent host phyla underscore the need for global, cross-species meta-analyses to capture the full diversity of coral virus-host interactions.

Text 3 (discussions)

Cui et al (2023)[13] summarized the first major step in resolving this paradox was the discovery that most of the TOC required by the coral for energy and biosynthesis is provided through their endosymbiotic dinoflagellate algae. A second major step was the recognition that the problem of limiting N can be solved by N conservation and/or recycling within the coral holobiont microbes.

Text 4 (discussions)

Beyond alleviating trace-element limitations, vAMGs also confer nutritional subsidies for macronutrients such as carbon, sulfur, and nitrogen. Photosynthetically fixed carbon, along with nitrogen assimilation and recycling, underpins the ecological success of coral metaorganisms. Yet, viral contributions to C/N assimilation remain poorly understood. Unraveling these mechanisms is critical for our understanding of holobiont functioning and ecological productivity. Some viruses present in freshwater were identified to carry AMGs involved in C metabolism, such as *pmoC* and *glnA*[14]. Here, we identified 85 CAZyme-associated vAMGs (Fig. 4B&C), highlighting the viral role in coral carbon cycling. These include glycosyltransferase 4 (*GT4*), which promotes polysaccharide synthesis; glycoside hydrolase 73 (*GH73*), which facilitates polysaccharide degradation; and glycogen metabolism genes (*glgA*/*P*), which regulate host glycogen storage and utilization, paralleling recent findings[8]. Previous, viruses are estimated to release at least 145 Gt of carbon annually by lysing prokaryotic cells in marine environment[15], which implying carbon cycling in coral ecosystem has also relies heavily on vAMGs. Viruses also contribute to sulfur metabolism: assimilatory

sulfate reduction genes (*cysE*/*K*/*Q*) enable cysteine biosynthesis under sulfur limitation, while dissimilatory sulfate reduction genes (*dsrC*/*E*) regulate sulfide production and redox balance. Moreover, CH_4 oxidation-related vAMGs (*acs*, *fwdB*, etc.) suggest viral enhancement of energy metabolism by enabling host exploitation of methane and other low-carbon compounds, thereby broadening carbon source diversity and supporting high reef productivity in coral reefs[6]. Nitrogen cycling presents a particularly compelling case. Nitrogen is the principal limiting nutrient on coral reefs, and recent work Cui et al.[13] confirmed that ammonium (NH_4^+) plays a central role in sustaining symbiont nitrogen conservation and recycling. Interestingly, although the overall number of vAMGs linked to nitrogen metabolism is low compared with other nutrient categories, *glnA* was markedly enriched (Fig. 4D). Given its pivotal role in nitrogen assimilation, this enrichment likely enhances microbial capacity to acquire and transform N sources, thereby supporting host adaptation to fluctuations in N supply or interspecific competition[16]. Collectively, these vAMGs suggest that viruses not only mitigate macronutrient constraints (C, N, P, S) but also fine-tune trace-element metabolism (e.g., Fe) in ways that sustain holobiont photosynthesis and growth under oligotrophic conditions. This provides a novel, virus-centred ecological framework for explaining Darwin's Paradox. Still, the relatively limited representation of nitrogen-related AMGs may reflect the host's tight regulation of nitrogen acquisition and recycling

.

The underlying mechanisms may include the following two aspects. Firstly, in coral reef ecosystem, the host functions more like a "farmer" managing "cows"[16]: it supplies the algae with abundant CO_2 ("feed") to drive photosynthesis, while limiting N ("fertilizer") to keep algal populations under control and ensure that most photosynthetic products-glucose ("milk") are transferred to the host rather than invested in algal growth. Under such a tightly regulated "farm" regime, N metabolism is already strictly controlled by the host, limiting the flow of N to bacteria. Consequently, phages originating from bacteria tend to have relatively fewer vAMGs encoding redundant N metabolic genes. Secondly, N metabolism involves energetically costly and enzyme-complex processes, such as nitrogenase activity, which is oxygen-sensitive and ATP-intensive, making direct viral intervention less favorable[6]. Instead, viruses may improve N utilization efficiency indirectly by targeting "bottleneck" nutrients such as P and Fe, which are essential cofactors for nitrogenase, thereby optimizing the host's N metabolism without directly encoding it. This resource-allocation trade-off allows viruses to dedicate limited genomic space toward functions with higher marginal returns in oligotrophic conditions, such as P and Fe acquisition.

References

1. Roux S, et al. Minimum information about an uncultivated virus genome (MIUViG). *Nat Biotechnol.* **37**, 29-37 (2019).
2. Bowers RM, et al. Minimum information about a single amplified genome (MISAG) and a metagenome-assembled genome (MIMAG) of bacteria and archaea. *Nat Biotechnol.* **35**, 725-731 (2017).
3. Guo, J. et al. VirSorter2: a multi-classifier, expert-guided approach to detect diverse DNA and RNA viruses. *Microbiome.* **9**, 37 (2021).

4. Nayfach, S., Camargo, A. P., Schulz, F., Eloe-Fadrosh, E., Roux, S., Kyrpides, N. C. CheckV assesses the quality and completeness of metagenome-assembled viral genomes. *Nat. Biotechnol*. **39**, 578–585 (2020).
5. Rubio-Portillo, E., Robertson, S., Antón, J. Coral mucus as a reservoir of bacteriophages targeting Vibrio pathogens. *ISME J*. **18**, 017 (2024).
6. Wiedenmann, J. et al. Reef-building corals farm and feed on their photosynthetic symbionts. *Nature*. **620**, 1018-1024 (2023).
7. Ferrier-Pagès, C., Sauzéat, L., Balter, V. Coral bleaching is linked to the capacity of the animal host to supply essential metals to the symbionts. *Global Change Biol*. **24**, 3145-3157 (2018).
8. Ji, M. et al. Biodiversity of mudflat intertidal viromes along the Chinese coasts. *Nat. Commun*. **15**, 8611 (2024).
9. Ma, B. et al. Biogeographic patterns and drivers of soil viromes. *Nat. Ecol & Evol*. **8**, 717–728 (2024).
10. Yang, J.H. et al. Host taxonomy and environment shapes insectivore viromes and viral spillover risks in Southwestern China. *Microbiome*. **13**, 122 (2025).
11. Wallace, B. A., Varona, N. S., Hesketh-Best, P. J., Stiffler, A. K., Silveira, C. B. Globally distributed bacteriophage genomes reveal mechanisms of tripartite phage–bacteria–coral interactions. *ISME J*. **18**, 132 (2024).
12. Cárdenas A, et al. Coral-associated viral assemblages from the central Red Sea align with host species and contribute to holobiont genetic diversity. *Front. Microbiol*, **30**, (2020).
13. Cui, G. et al. Molecular insights into the Darwin paradox of coral reefs from the sea anemone Aiptasia. *Sci. Adv*. **9**, 7108 (2023).
14. Chen, L.X. et al. Large freshwater phages with the potential to augment aerobic methane oxidation. *Nat. Microbiol*. **5**, 1504-1515 (2020).
15. Lara, E. et al. Unveiling the role and life strategies of viruses from the surface to the dark ocean. *Sci. Adv*. **3**, e1602565 (2017).
16. Matz, M. V. Not-so-mutually beneficial coral symbiosis. *Current Biol*. **34**, R798-R801 (2024).

Supplementary Figures

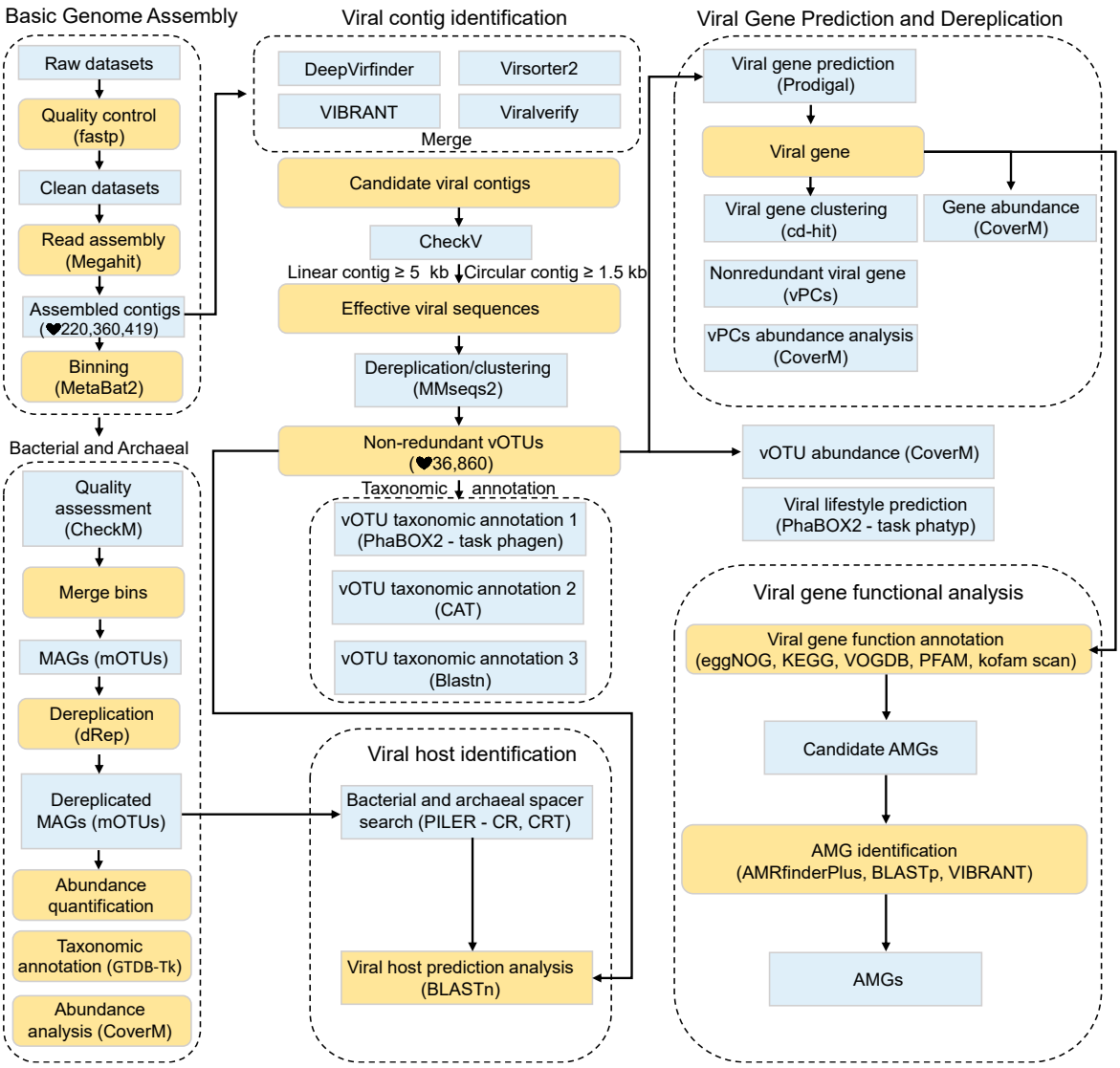

Supplementary Figure 1. Metagenomic analysis pipeline for metagenome-assembled genome (MAG) recovery, viral contig identification, and taxonomic classification. The primary analysis tools and the count of viral contigs or MAGs are delineated on the diagram. AMG: auxiliary metabolic gene; vOTU: viral operational taxonomic unit; vPC: viral gene set.

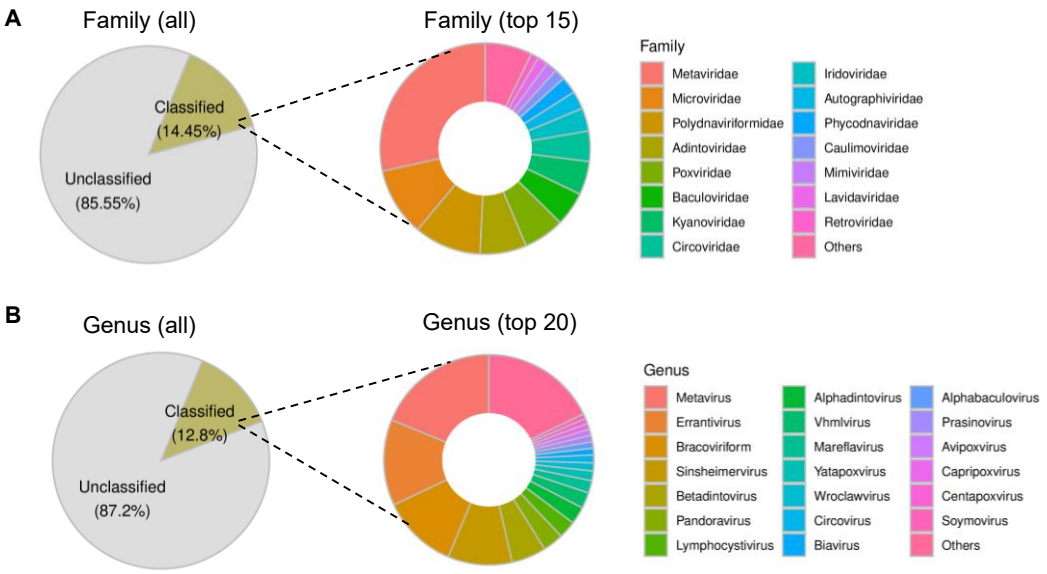

Supplementary Figure 2. Taxonomic classification of viruses at the family and genus levels in the GCVHD. Taxonomic classification of viruses at the family level (A) and genus level (B), respectively. The left panel depicts the proportion of classified versus unclassified viruses, while the right panel illustrates the composition of the top 15 viral families and top 20 genera within the taxonomically classified fraction.

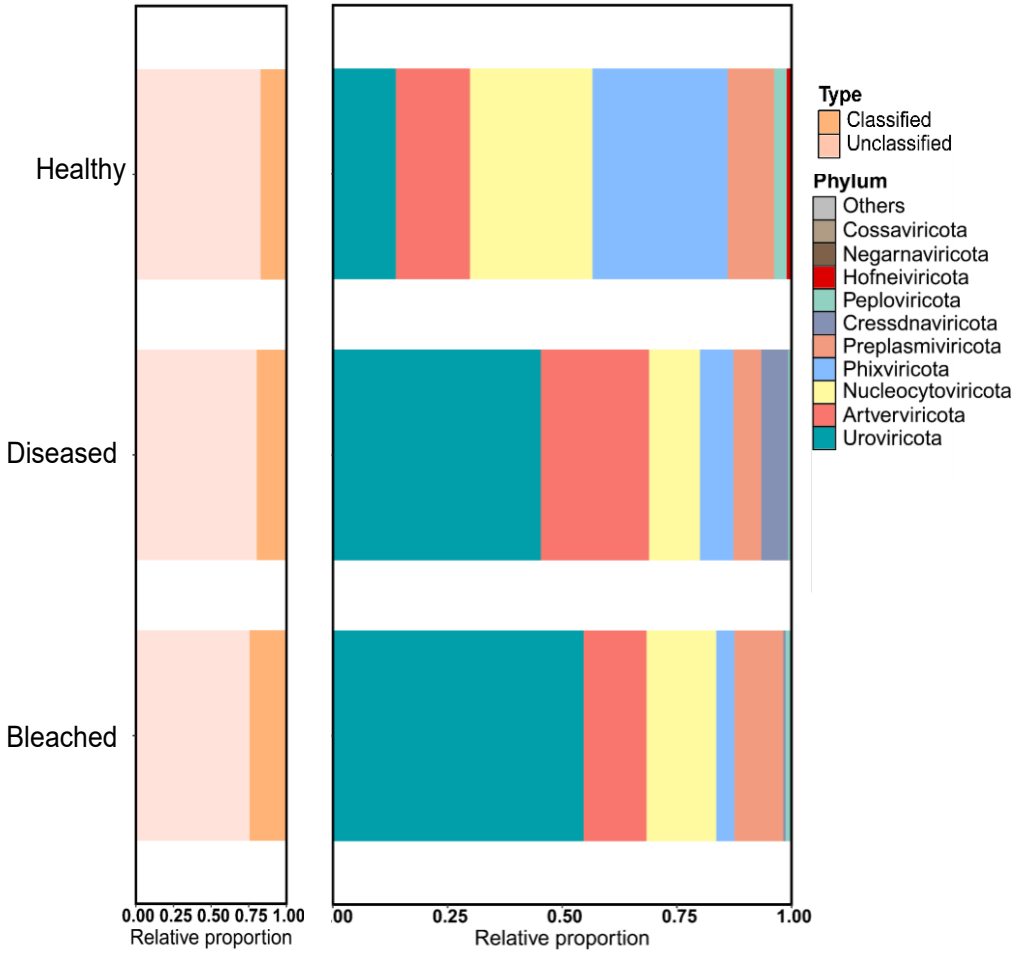

Supplementary Figure 3. Distribution of classified and unclassified viruses (left) and community composition (right) of viruses at the phylum level among different coral health status. All samples were classified as healthy, diseased, and bleached in the GCVHD.

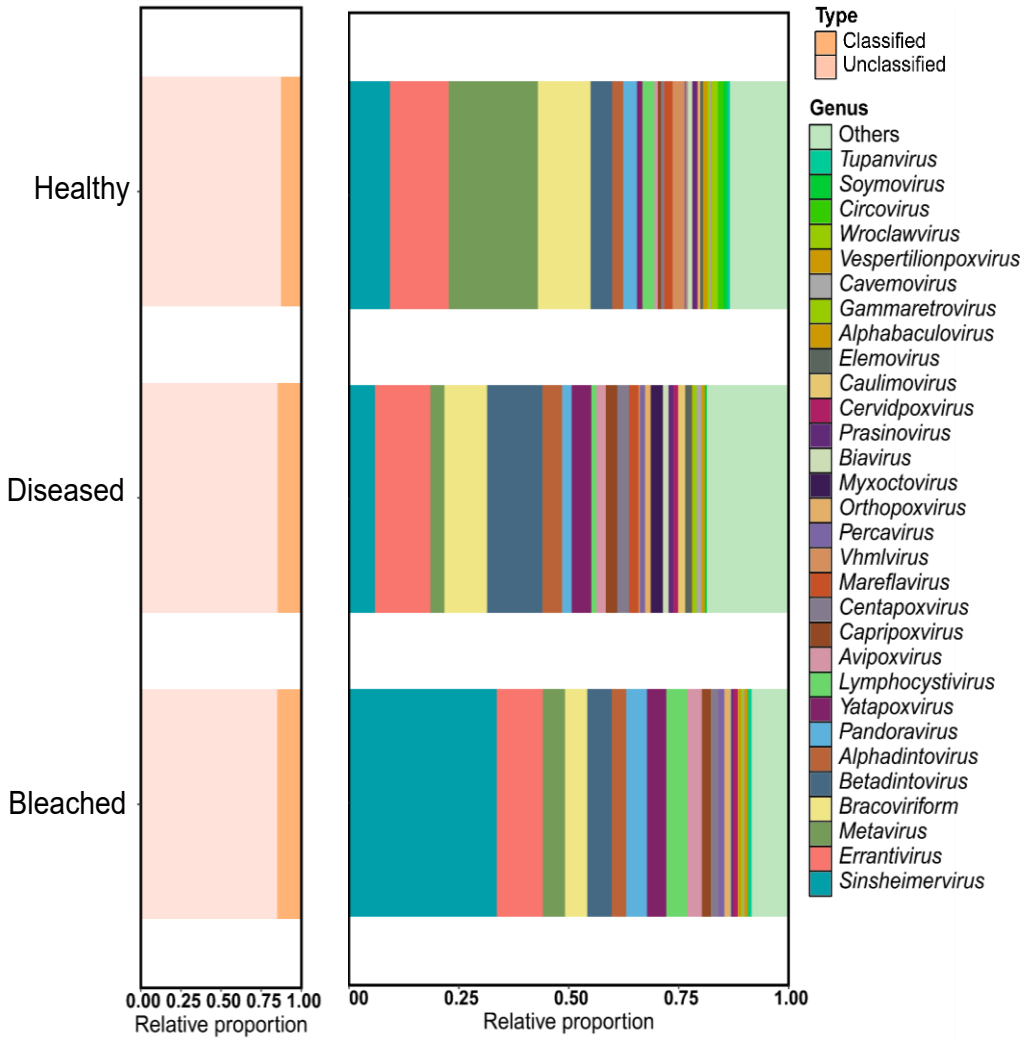

Supplementary Figure 4. Distribution of classified and unclassified viruses (left) and community composition (right) of viruses at the genus level among different coral health status. All samples were classified as healthy, diseased, and bleached in the GCVHD.

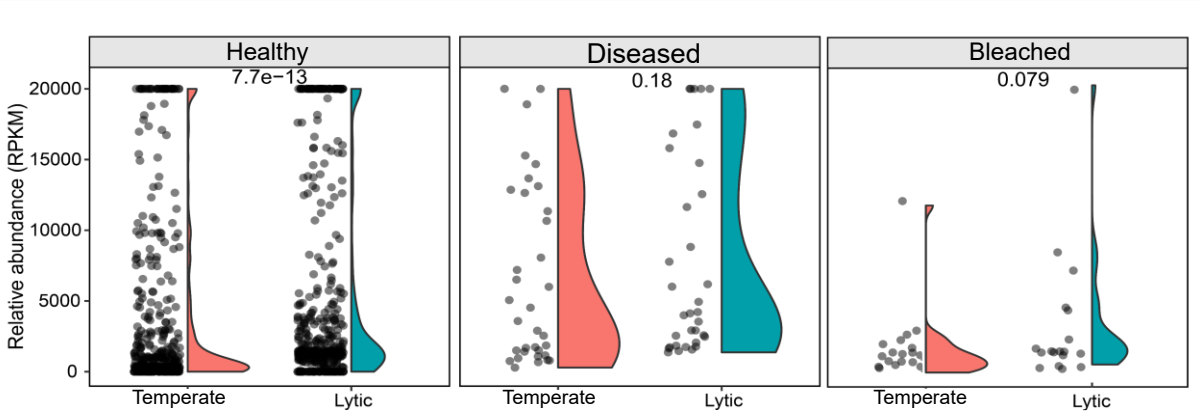

Supplementary Figure 5. Relative abundance (expressed as RPKM) of lytic and temperate viruses, stratified by coral health status. All samples were classified as healthy, diseased, and bleached in the GCVHD.

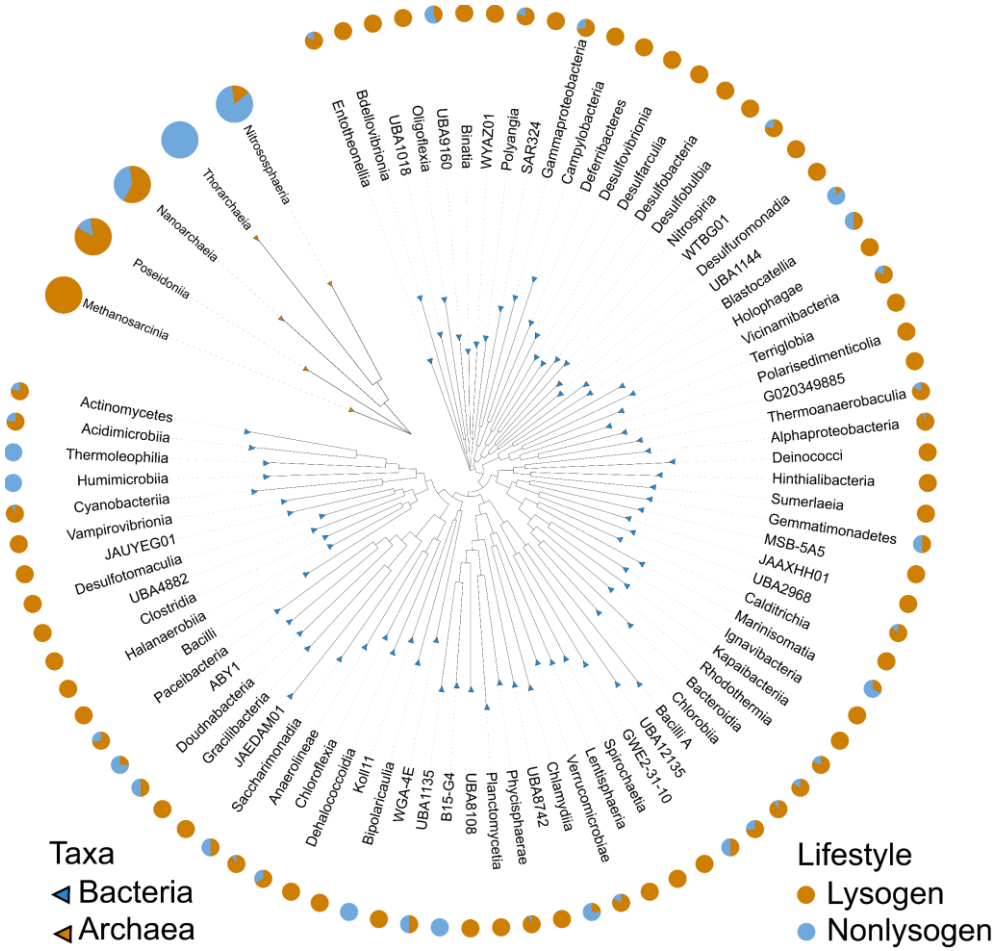

Supplementary Figure 6. Ratios of lysogeny prokaryotic taxa in GCVGD. The bacterial and archaeal phylogenetic trees were constructed based on concatenated marker proteins, respectively, using the maximum-likelihood algorithm.

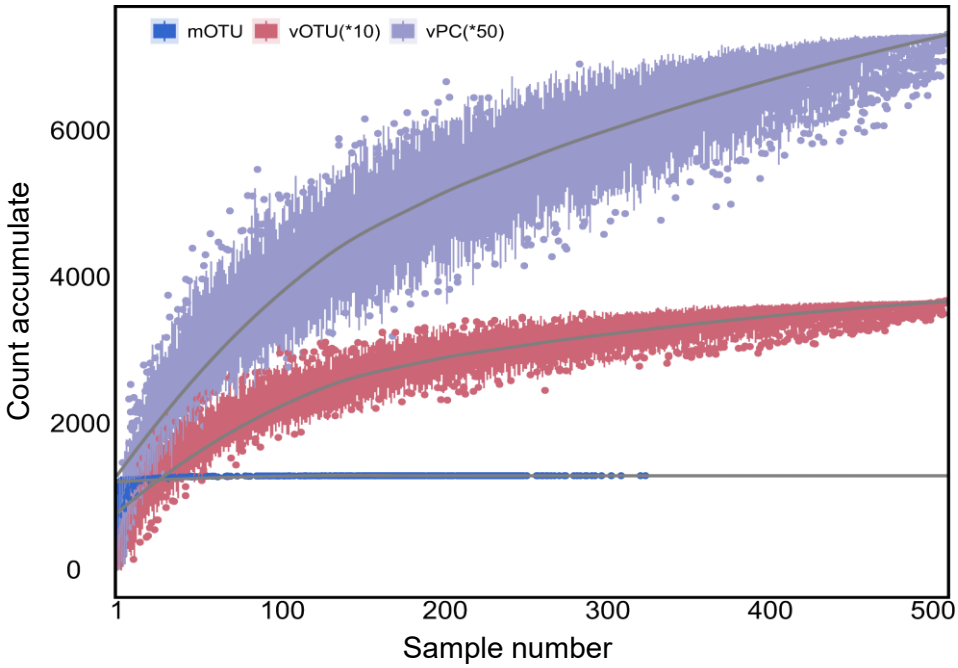

Supplementary Figure 7. Accumulation curves of vOTUs (pink), mOTUs (blue), and vPCs (purple) with mean±SEM plotted dots.

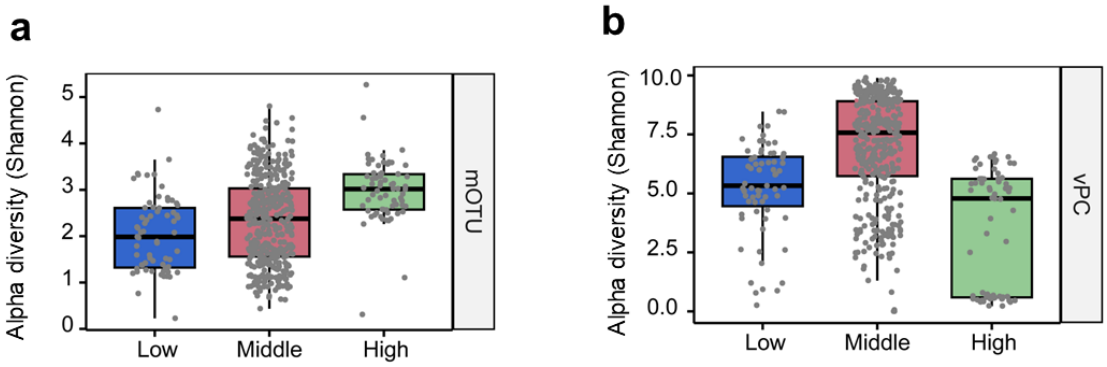

Supplementary Figure 8. The alpha diversity (Shannon) of prokaryotes (mOTUs) and viral genes (vPCs) and across different latitude (low <15°, medium 15°-25°, and high >25°). The points represent the richness of each sample. The center lines of the boxes indicate the median. The bounds of the box represent the interquartile range, with the lower bound corresponding to the first quartile and the upper bound to the third quartile.

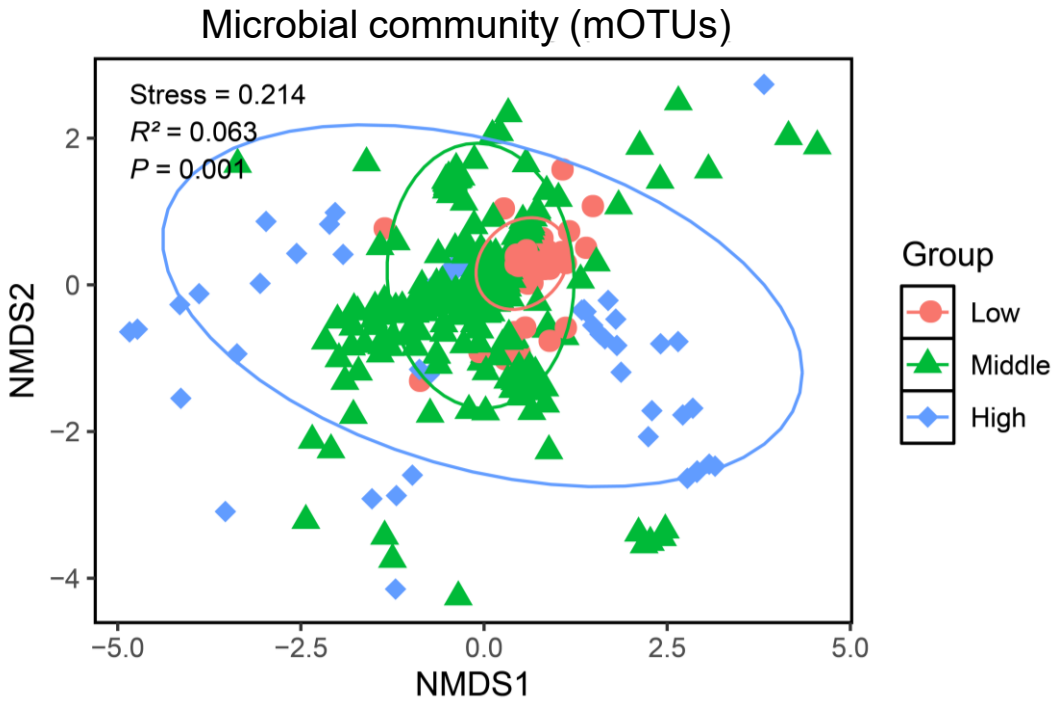

312
313
314 **Supplementary Figure 9. Nonmetric multidimensional scaling analyses of microbial**
315 **communities based on BrayCurtis distance.** Different colors represent samples from different
316 latitudes (low, middle, and high). The significance between sampling sites was assessed using
317 analysis of similarity with 999 permutations.
318

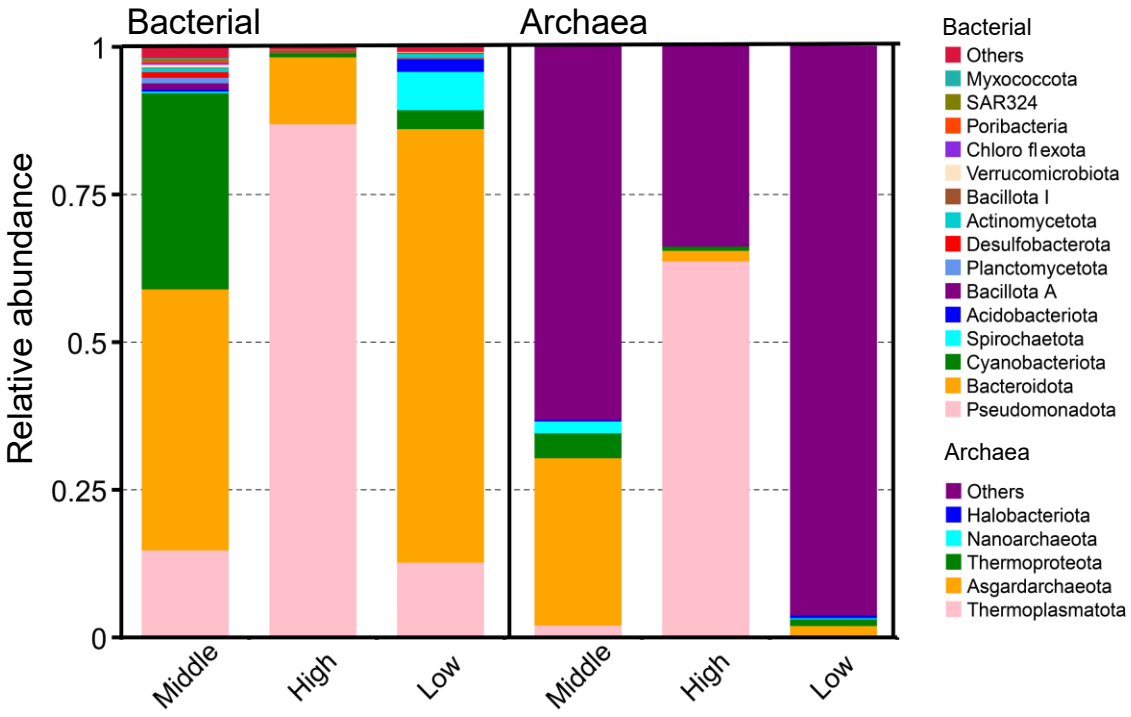

Supplementary Figure 10. The relative proportions of bacterial and archaeal taxa at phylum level, stratified by coral latitude. All samples were classified as middle, high, and low in the GCVHD.

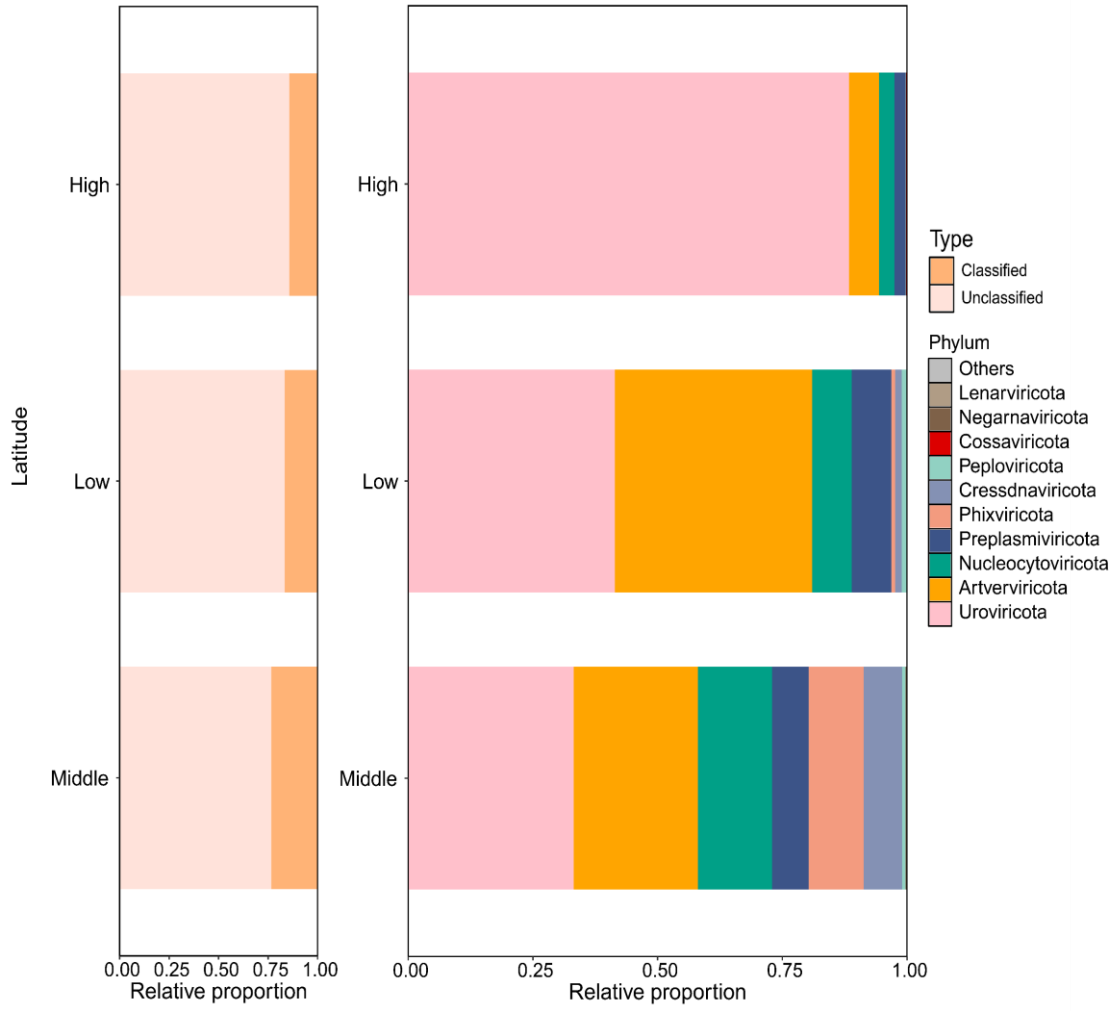

Supplementary Figure 11. Distribution of classified and unclassified viruses (left) and community composition of viruses (right) at the phylum level among different latitude.

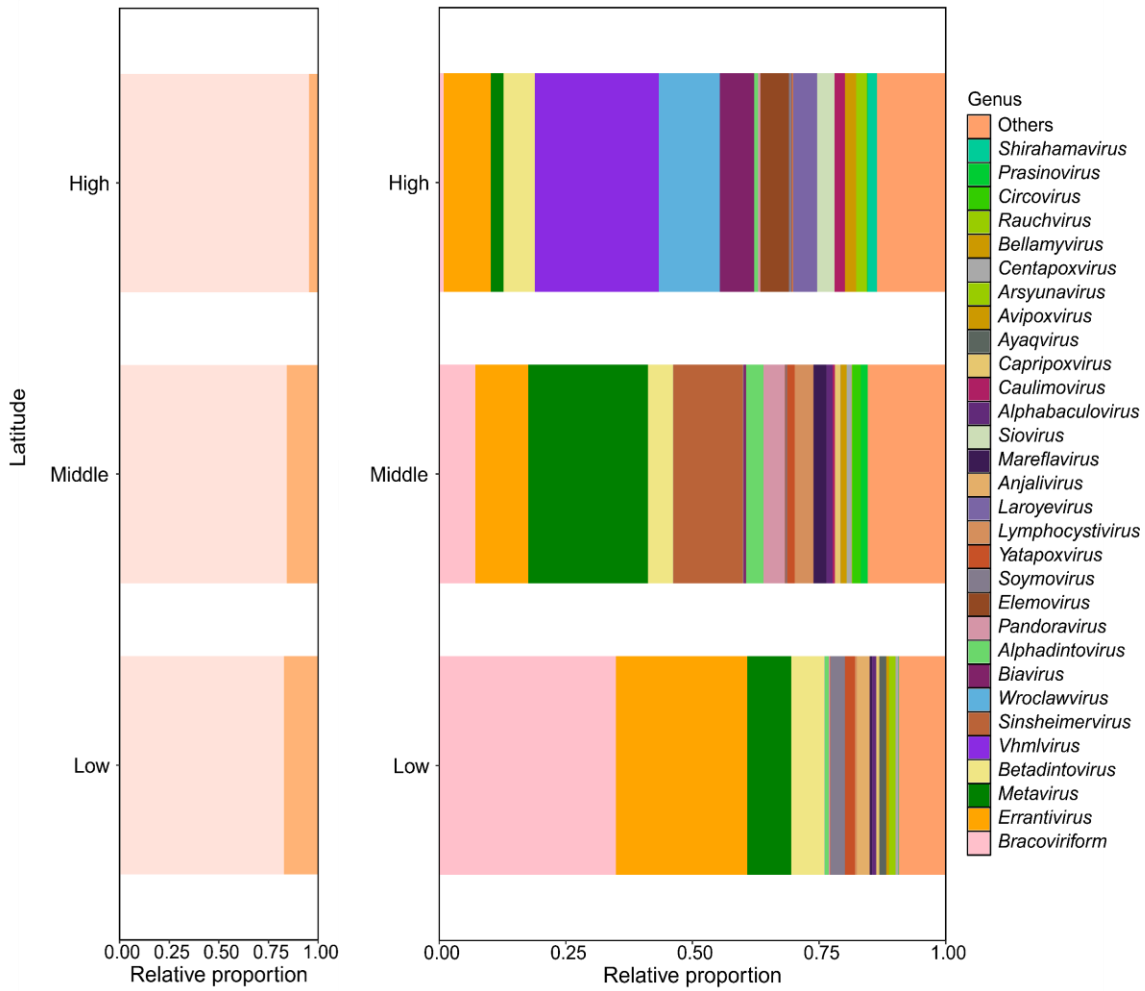

Supplementary Figure 12. Distribution of classified and unclassified viruses (left) and community composition of viruses (right) at the genus level among different latitude.

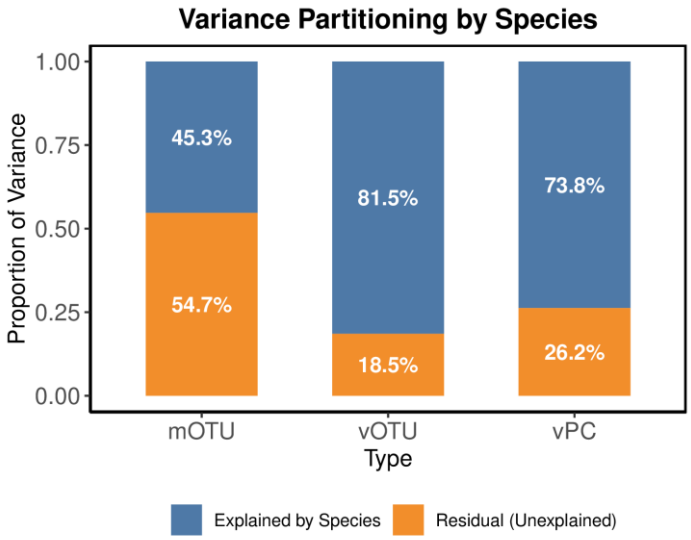

Supplementary Figure 13. Variance partitioning of community variation across microbial and viral taxonomic/functional units (mOTU, vOTU, vPC). The stacked bar chart displays the results of variance partitioning for community variation corresponding to microbial operational taxonomic units (mOTU), viral operational taxonomic units (vOTU), and viral protein clusters (vPC). The blue segment represents the proportion of variance explained by species, while the orange segment represents the residual (unexplained variance).

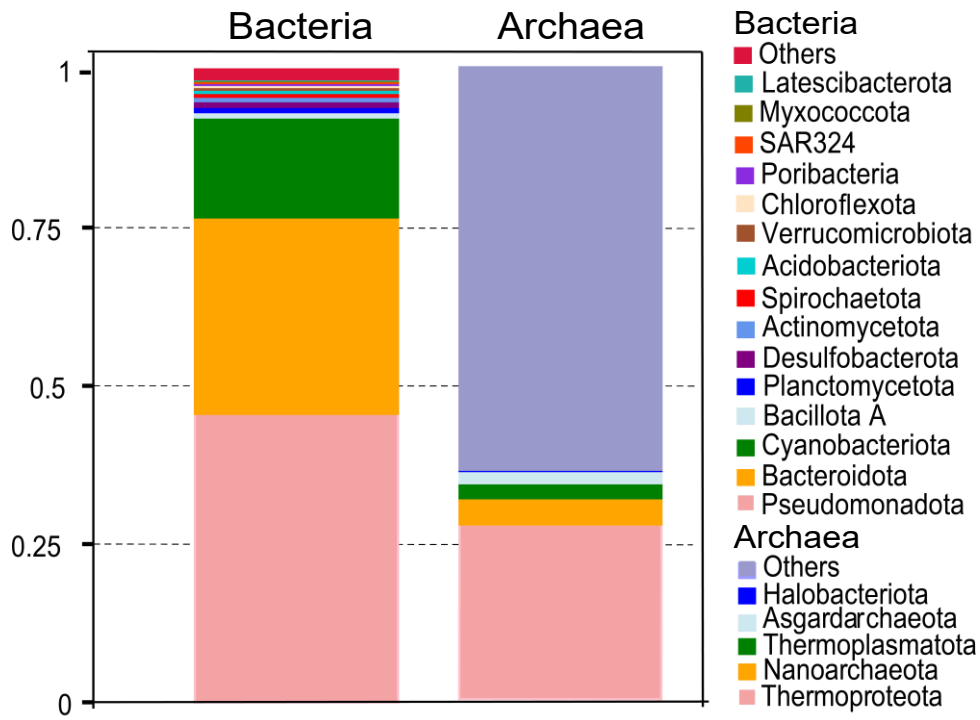

Supplementary Figure 14. The relative proportions of bacterial and archaeal taxa at phylum level.

Supplementary Figure 15. The relative proportions of bacterial and archaeal taxa at phylum level in different groups, stratified by coral health status.

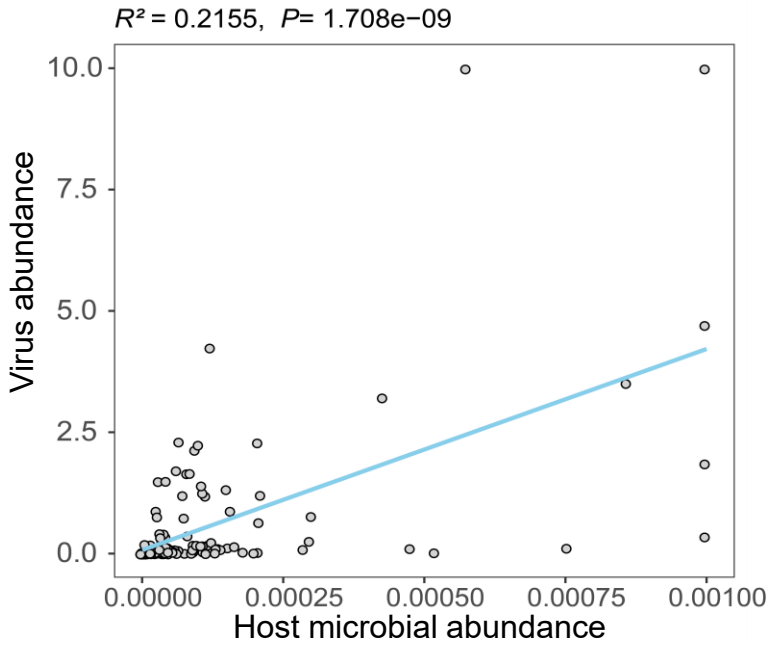

Supplementary Figure 16. The relationship between normalized viral and host microbial abundance. The best polynomial fit was determined between first- and second-order polynomial fits based on the corrected Akaike Information Criterion (AICc). The R^2 values represent the proportion of variance explained by the polynomial regression model.

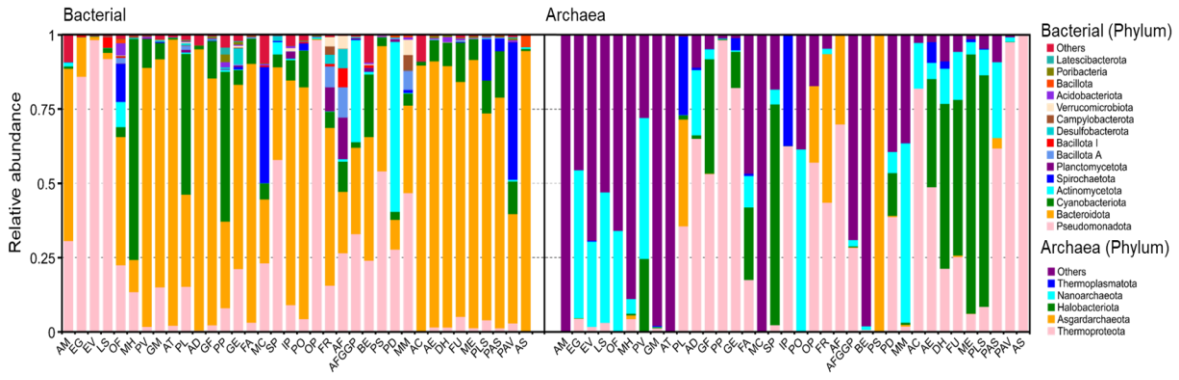

Supplementary Figure 17. The relative proportions of bacterial and archaeal taxa at phylum level, stratified by coral species. Coral species name: AC: *Acropora cytherea*; AD: *Acropora digitifera*; AE: *Acanthastrea echinata*; AF: *Acropora Formosa*; AFGGP: *Acropora tenuis*, *Fungia fungites*, *Goniastrea aspera*, *Galaxea fascicularis* and *Pocillopora verrucosa*; AM: *Acropora muricata*; AS: *Acropora aspera*; AT: *Acropora tenuis*; BE: *Balanophyllia europaea*; DH: *Diploastrea heliopore*; EG: *Eunicella gazella*; EV: *Eunicella verrucosa*; FA: *Favites abdita*; FR: *Fungia repanda*; FU: *Fungia* sp.; GE: *Goniastrea edwardsi*; GF: Galaxea fascicularis; GM: *Goniastrea minuta*; IP: *Isopora palifera*; LS: *Leptogorgia sarmentosa*; MC: *Montastraea cavernosa*; ME: *Mycedium elephantotus*; MH: *Montipora hispida*; MM: *Meandrina meandrites*; OF: *Orbicella faveolate*; OP: *Oculina patagonica*; PAS: *Pachyseris speciosa*; PAV: *Pavona varians*; PD: *Pocillopora damicornis*; PL: *Porites lutea*; PLS: *Plerogyra sinuosa*; PO: *Pocillopora*; PP: *Porites pukoensis*; PS: *Pseudodiploria strigose*; PV: *Pocillopora verrucosa*; SP: *Stylophora pistillata*.

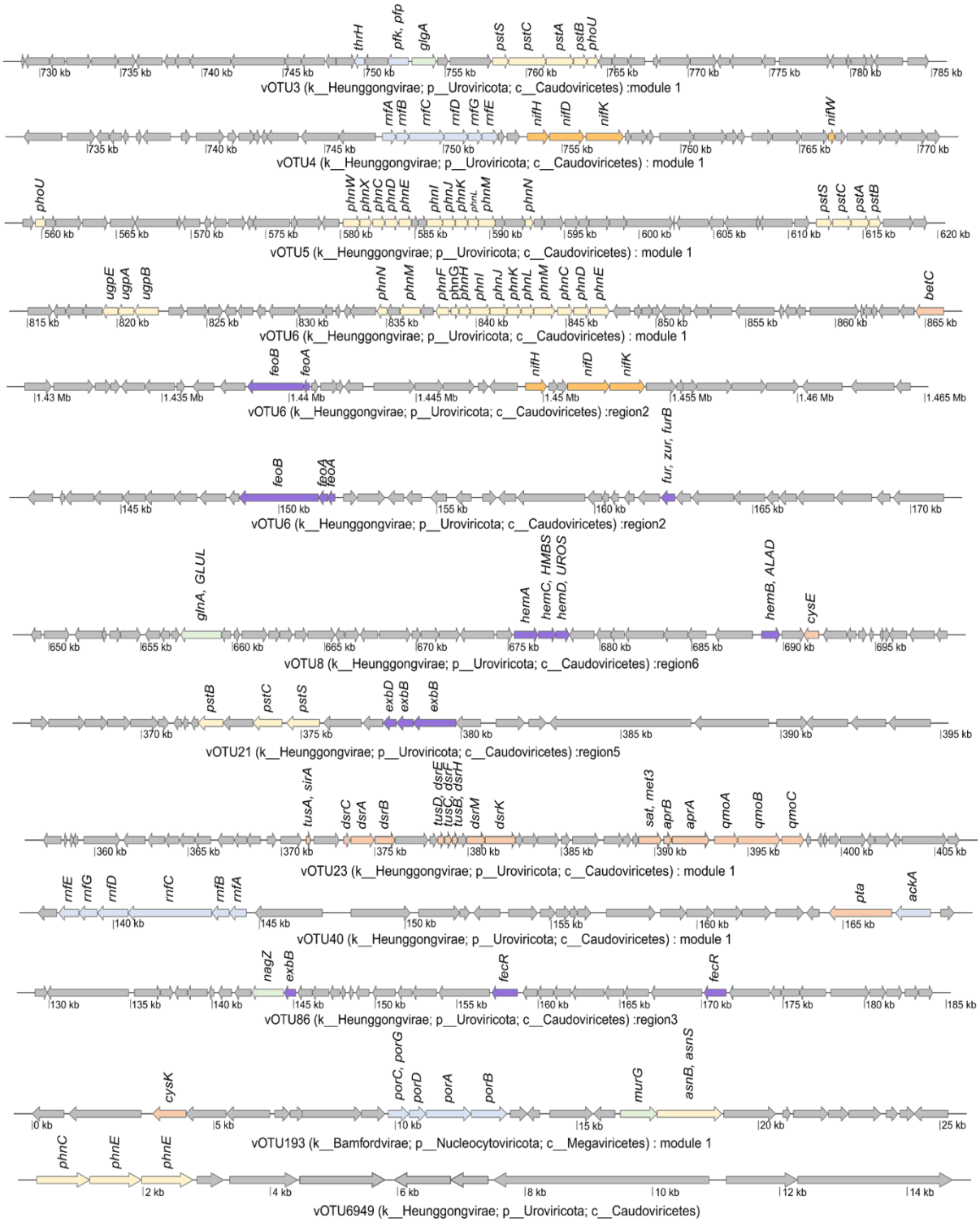

Supplementary Figure 18. Comparative genomic analysis of viral AMGs. Only genes with > 90% identity and > 90% coverage were concatenated. Source data are provided as a Source Data file.

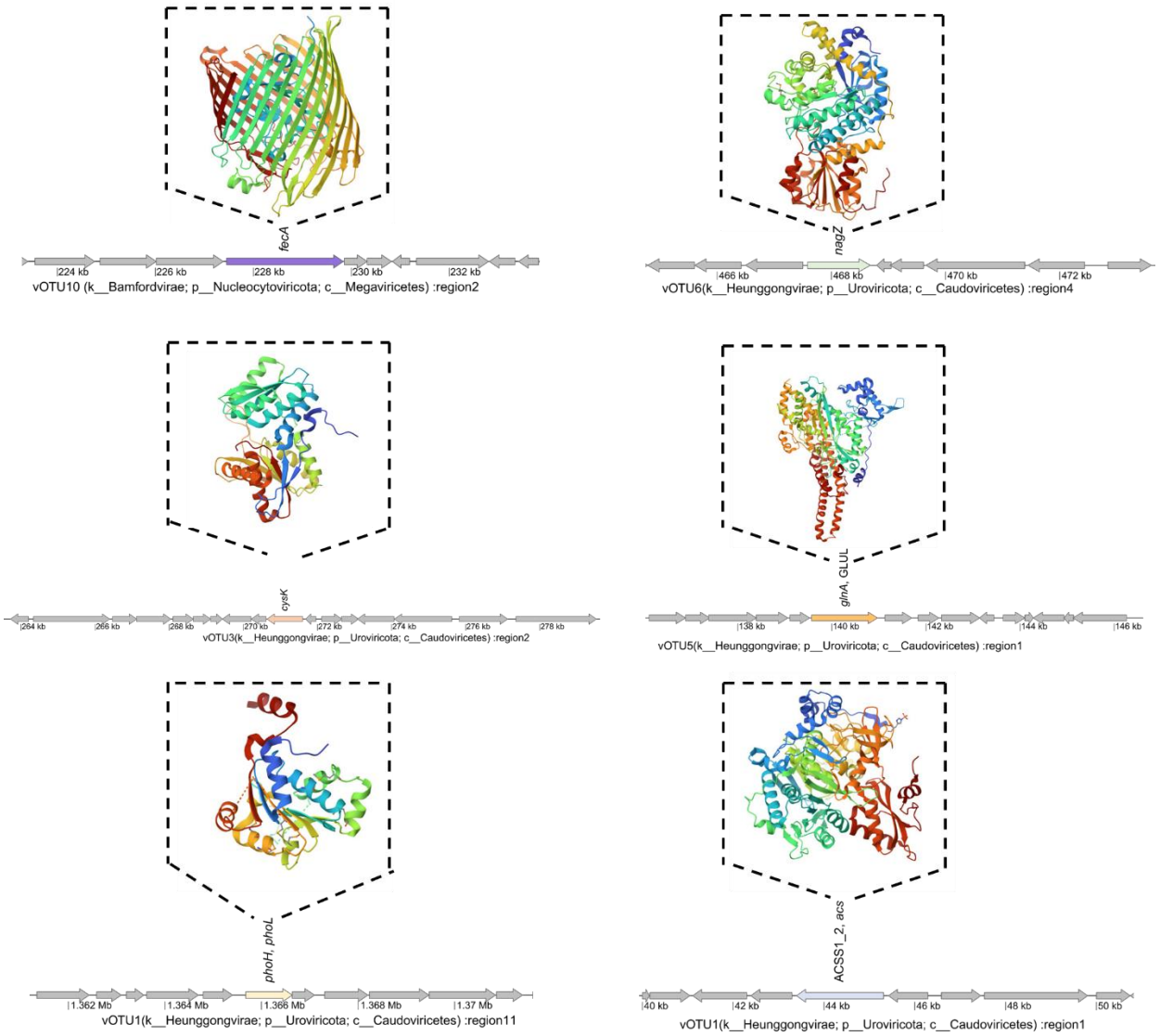

Supplementary Figure 19. Three-dimensional structure prediction and genomic localization of typical vAMGs. Three-dimensional protein structures of six vAMGs (upper half) and their location information in the corresponding vOTUs (lower half).

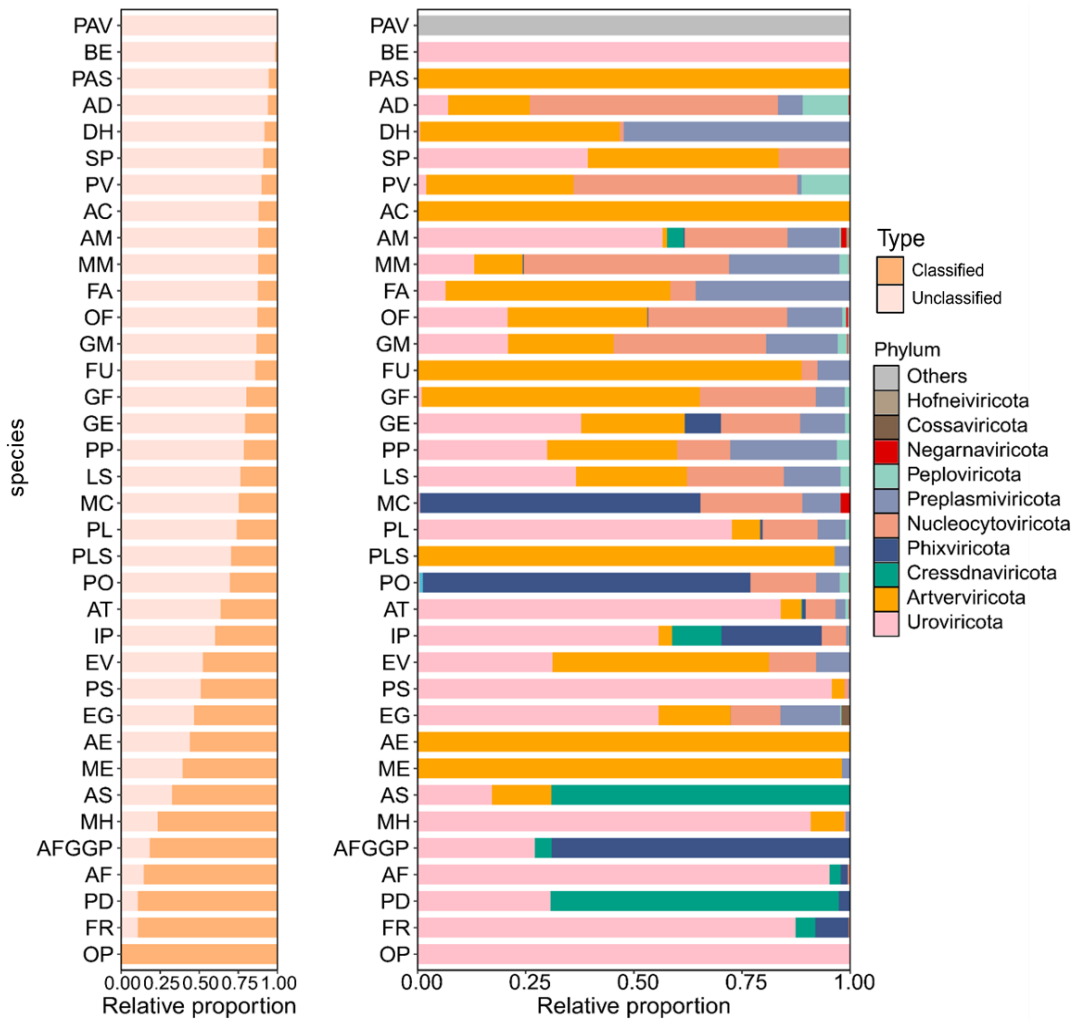

Supplementary Figure 20. Distribution of classified and unclassified viruses (left) and viral composition at the phylum level among different coral species (right). Coral species name: AC: *Acropora cytherea*; AD: *Acropora digitifera*; AE: *Acanthastrea echinata*; AF: *Acropora Formosa*; AFGGP: *Acropora tenuis*, *Fungia fungites*, *Goniastrea aspera*, *Galaxea fascicularis* and *Pocillopora verrucosa*; AM: *Acropora muricata*; AS: *Acropora aspera*; AT: *Acropora tenuis*; BE: *Balanophyllia europaea*; DH: *Diploastrea heliopore*; EG: *Eunicella gazella*; EV: *Eunicella verrucosa*; FA: *Favites abdita*; FR: *Fungia repanda*; FU: *Fungia* sp.; GE: *Goniastrea edwardsi*; GF: Galaxea fascicularis; GM: *Goniastrea minuta*; IP: *Isopora palifera*; LS: *Leptogorgia sarmentosa*; MC: *Montastraea cavernosa*; ME: *Mycedium elephantotus*; MH: *Montipora hispida*; MM: *Meandrina meandrites*; OF: *Orbicella faveolate*; OP: *Oculina patagonica*; PAS: *Pachyseris speciosa*; PAV: *Pavona varians*; PD: *Pocillopora damicornis*; PL: *Porites lutea*; PLS: *Plerogyra sinuosa*; PO: *Pocillopora*; PP: *Porites pukoensis*; PS: *Pseudodiploria strigose*; PV: *Pocillopora verrucosa*; SP: *Stylophora pistillata*.

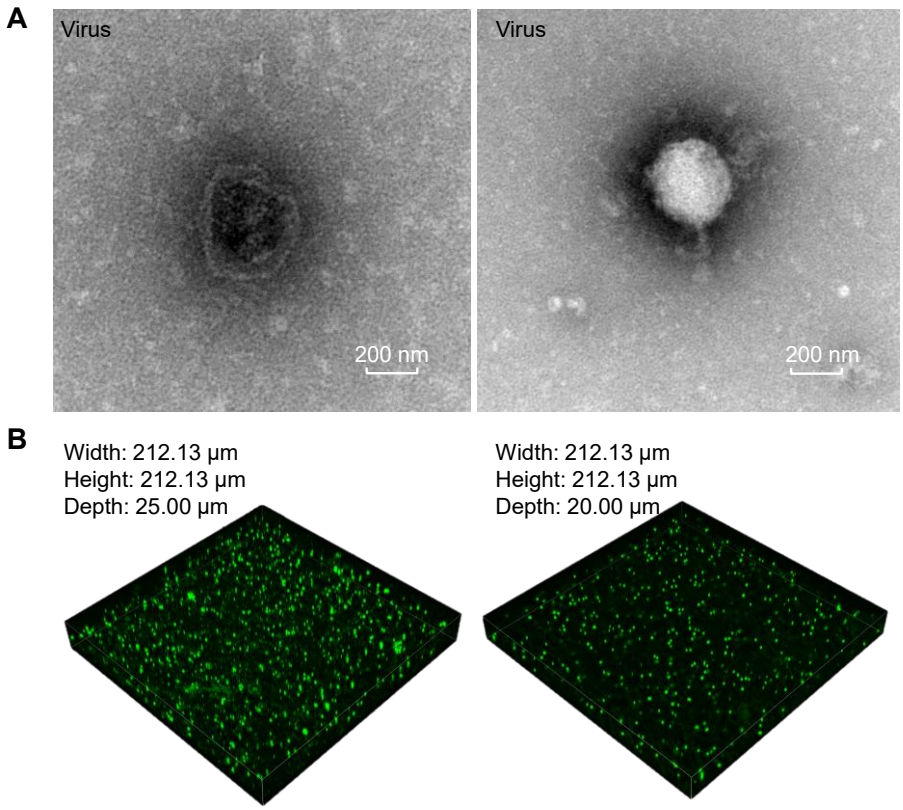

Supplementary Figure 21. Transmission electron microscopic and laser scanning confocal microscopy images of viral particles extracted from *A. digitifera*. Laser scanning confocal microscopy images (b, left: VH and right: VL) from a coral sample filtered onto a Whatman 0.02 mm Anodisc filter stained with SYBR Gold.

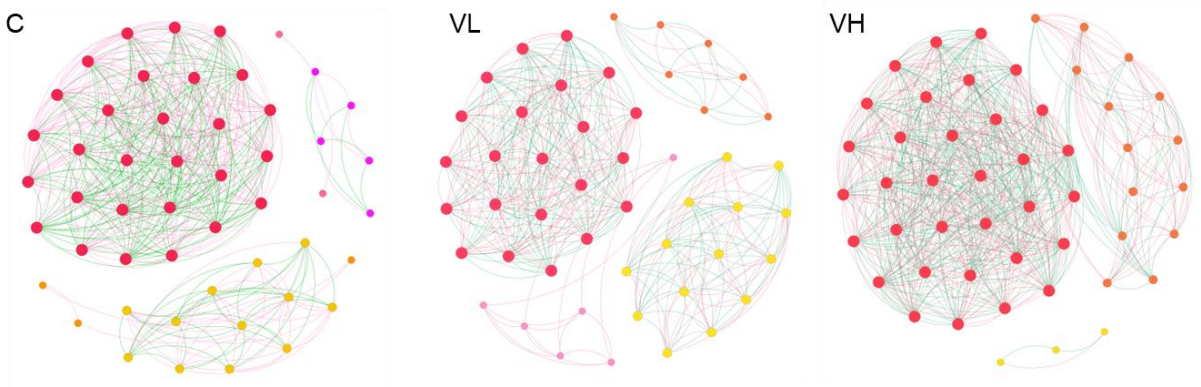

Supplementary Figure 22. Co-occurrence networks of prokaryotic communities at the genus level. Genera occurring in over 10% of samples were included in the networks. Edges were selected using a correlation coefficient >|0.7| and a p-value of <0.01 as the criteria. The size of each node corresponds to the number of significant correlations for that genus.

Supplementary Data 1 to 17 (Excel):

Supplementary Data 1. The coral metagenomes and viromes analyzed in this study

Supplementary Data 2. Sequencing information in our data in this study

Supplementary Data 3. Viral operational taxonomic unit taxonomy in this study

Supplementary Data 4. Viral lifestyle analyzed in this study

Supplementary Data 5. Lysogeny in prokaryotes analyzed in this study

Supplementary Data 6. Viral genomic completeness analyzed in this study

Supplementary Data 7. The viral clusters analyzed in this study

Supplementary Data 8. Multi-habitat analyzed in this study

Supplementary Data 9. Virus-host association analyzed in this study

Supplementary Data 10. The prokaryotes analyzed in this study

Supplementary Data 11. The virus-to-host ratio analyzed in this study

Supplementary Data 12. Virus-host network relationship analyzed in this study

Supplementary Data 13. Viral functional genes analyzed in this study

Supplementary Data 14. The viral auxiliary metabolic genes analyzed in this study

Supplementary Data 15. Classification analysis of viral auxiliary metabolic genes in this study

Supplementary Data 16. Key screening analysis of viral auxiliary metabolic genes in this study

Supplementary Data 17. Network analysis of prokaryotes following viral treatment in this study